Triazole-derivatized near-infrared cyanine dyes enable local functional fluorescent imaging of ocular inflammation

Thomas, Chloe; Alfahad, Nada; Capewell, Nicholas; Cowley, Jamie; Hickman, Eleanor; Fernandez, Antonio; Harrison, Neale; Qureshi, Omar; Bennett, Naomi; Barnes, Nicholas; Dick, Andrew; Chu, Colin; Liu, Xiaoxuan; Denniston, Alastair; Vendrell, Marc; Hill, Lisa J

DOI:
10.1016/j.bios.2022.114623

Biosensors and Bioelectronics 216 (2022) 114623

Contents lists available at ScienceDirect

Biosensors and Bioelectronics

journal homepage: www.elsevier.com/locate/bios

Triazole-derivatized near-infrared cyanine dyes enable local functional fluorescent imaging of ocular inflammation

Chloe N. Thomas [a,*], Nada Alfahad [b], Nicholas Capewell [c], Jamie Cowley [d], Eleanor Hickman [a], Antonio Fernandez [e,f], Neale Harrison [d], Omar S. Qureshi [d], Naomi Bennett [a,g], Nicholas M. Barnes [h], Andrew D. Dick [i,j], Colin J. Chu [i,j], Xiaoxuan Liu [b,c,k,l], Alastair K. Denniston [b,c,i,k,l,m], Marc Vendrell [f], Lisa J. Hill [a,*]

[a] School of Biomedical Sciences, Institute of Clinical Sciences, College of Medical and Dental Sciences, University of Birmingham, Birmingham, UK
[b] Institute of Inflammation and Ageing, University of Birmingham, Birmingham, UK
[c] University Hospitals Birmingham NHS Foundation Trust, Birmingham, UK
[d] Celentyx Ltd, Birmingham Research Park, Vincent Drive, Edgbaston, Birmingham, UK
[e] Department of Organic Chemistry, Faculty of Chemistry, University of Murcia, Murcia, Spain
[f] Centre for Inflammation Research, Queen's Medical Research Institute, The University of Edinburgh, Edinburgh, UK
[g] Healthcare Technologies Institute, School of Chemical Engineering, University of Birmingham, Birmingham, UK
[h] Neuropharmacology Research Group, Institute of Clinical Sciences, College of Medical and Dental Sciences, University of Birmingham, Edgbaston, Birmingham, UK
[i] National Institute for Health Research (NIHR) Biomedical Research Centre at Moorfields Eye Hospital and University College London Institute of Ophthalmology, London, UK
[j] Academic Unit of Ophthalmology, Bristol Medical School and School of Cellular and Molecular Medicine, University of Bristol, Bristol, UK
[k] Birmingham Health Partners Centre for Regulatory Science and Innovation, University of Birmingham, Birmingham, UK
[l] Health Data Research UK, London, UK
[m] Centre for Patient Reported Outcomes Research, Institute of Applied Health Research, University of Birmingham, Birmingham, UK

ARTICLE INFO

Keywords:
Near-infrared
Fluorophores
Cyanine
Uveitis
Optical coherence tomography
Leukocytes

ABSTRACT

Near-infrared (NIR) chemical fluorophores are promising tools for *in-vivo* imaging in real time but often succumb to rapid photodegradation. Indocyanine green (ICG) is the only NIR dye with regulatory approval for ocular imaging in humans; however, ICG, when employed for applications such as labelling immune cells, has limited sensitivity and does not allow precise detection of specific inflammatory events, for example leukocyte recruitment during uveitic flare-ups. We investigated the potential use of photostable novel triazole NIR cyanine (TNC) dyes for detecting and characterising activated T-cell activity within the eye. Three TNC dyes were evaluated for ocular cytotoxicity *in-vitro* using a MTT assay and optimised concentrations for intraocular detection within *ex-vivo* porcine eyes after topical application or intracameral injections of the dyes. TNC labelled T-cell tracking experiments and mechanistic studies were also performed *in-vitro*. TNC-1 and TNC-2 dyes exhibited greater fluorescence intensity than ICG at 10 μM, whereas TNC-3 was only detectable at 100 μM within the porcine eye. TNC dyes did not demonstrate any ocular cell toxicity at working concentrations of 10 μM. $CD4^+$T-cells labelled with TNC-1 or TNC-2 were detected within the porcine eye, with TNC-1 being brighter than TNC-2. Detection of TNC-1 and TNC-2 into $CD4^+$T-cells was prevented by prior incubation with dynole 34–2 (50 μM), suggesting active uptake of these dyes via dynamin-dependent processes. The present study provides evidence that TNC dyes are suitable to detect activated $CD4^+$T-cells within the eye with potential as a diagnostic marker for ocular inflammatory diseases.

* Corresponding authors. School of Biomedical Sciences, Institute of Clinical Sciences, College of Medical and Dental Sciences, University of Birmingham, Birmingham, B15 2TT, UK.

E-mail addresses: c.thomas.4@bham.ac.uk (C.N. Thomas), l.j.hill@bham.ac.uk (L.J. Hill).

https://doi.org/10.1016/j.bios.2022.114623
Received 14 April 2022; Received in revised form 28 July 2022; Accepted 3 August 2022
Available online 13 August 2022

1. Introduction

Intraocular inflammation is the pathological hallmark of a number of sight-threatening intraocular inflammatory conditions, collectively known clinically as 'uveitis'. Patients may experience a range of symptoms including pain, light sensitivity, disturbances in vision and reduction in visual acuity. Uveitis is the third greatest cause of visual loss globally, accounting for 10–15% of all blindness in developed countries (de Boer et al., 2003). Uveitis primarily affects people of working age (20–50 years of age) and has important socio-economic consequences (Lardenoye et al., 2006; Jalil et al., 2012). Effective diagnosis, monitoring and assessment of treatment response is dependent predominantly on visualisation of the inflammatory cells within the eye. Traditionally this was done with various types of binocular microscope (notably the 'slit lamp'), which provide sufficient resolution to visualise individual inflammatory cells in the anterior chamber and vitreous cavity of the eye but not in the posterior structures such as the retina or choroid, where sight-threatening damage occurs. Hospital eye services now routinely provide multimodal imaging platforms incorporating optical coherence tomography (OCT) with resolution of the posterior structures of the eye down to a few microns, three-dimensional reconstructions, objective quantification, potential automation and the recording and registration to a reference image enabling reliable longitudinal comparison. One particular scanning laser ophthalmoscopy based multimodal system is the widely used SPECTRALIS® from Heidelberg Engineering which in addition to OCT, can include dye-based angiography, both fluorescein and indocyanine green (ICG). Both clinical and OCT techniques to assess disease activity in uveitis have focused on the *quantity* of the key inflammatory signs, such as the number of inflammatory cells visualised or the volume of oedema within the central retina ('cystoid macular oedema') (Jabs et al., 2005). So far assessment of the *nature* of the inflammation, specifically the cell type at any particular location and particularly at tissue sites within the eye has been out of reach in human patients. Categorising the type and extent of infiltrating cells and their distribution within the eye would dramatically accelerate our understanding of many of the sight-threatening forms of uveitis (most of which do not have an animal model), and would enable faster, more accurate diagnosis and the ability to monitor disease regression or relapse more sensitively.

Near-infrared (NIR) fluorophores are powerful tools for *in-vivo* imaging because they allow deep tissue penetration with minimal photodamage and low tissue autofluorescence (Vendrell et al., 2011; Fernandez et al., 2017; Benson et al., 2019; Cheng et al., 2020; Scott et al., 2021). NIR fluorophores have been described for multiple imaging applications, spanning from *in-vitro* analyte detection to *in-vivo* image-guided surgery (Yraola et al., 2004; Samanta et al. 2010, 2011; Park et al., 2014; Wu et al., 2019; Curtin et al., 2021). Notably, NIR fluorophores tend to be susceptible to chemical modification to fine-tune their optical and targeting properties. Their versatility has allowed utility to visualise real-time endogenous nitroxyl (Huang et al., 2019), selenocysteine production from mitochondria (Han et al., 2018) (Han et al., 2017), cellular carbon monoxide (Li et al., 2021), chlorine monoxide (Cao et al., 2019) and brain ozone (Li et al., 2019) in murine models of inflammation. The diversification of NIR cyanines has been exploited for structure-inherent targeting of different tissues (Hyun et al. 2014, 2015), and zwitterionic heptamethine cyanines have also been described as NIR agents with enhanced capabilities for cell, tissue and *in-vivo* imaging (Thavornpradit et al., 2019). Specific immune cell labelling for T-cell membranes (Kwon et al., 2021), intracellular signalling (Pacheco et al., 2013) or T-cell activators (e.g. granzymes) (He et al., 2020) have been achieved using NIR dyes demonstrating their functionality for specific immune cell labelling (Mendive-Tapia and Vendrell, 2022). However, despite recent advances, ICG is the only NIR dye with regulatory approval for use in humans, (Sakka, 2007; Luciano et al., 2019). In ophthalmology clinics, ICG is injected intravenously to detect blood flow or gross tissue abnormalities in the eye's choroid. ICG is generally safe when administered systemically and is cleared quickly by the liver (Alander et al., 2012); however it degrades swiftly upon light irradiation and is toxic to retinal pigment epithelium (RPE) (Penha et al., 2013; Awad et al., 2018; Sato et al., 2018). As ICG is a negatively-charged structure it has a high affinity to bind plasma proteins, is mainly retained in intravascular spaces and is unable to label immune cells specifically (Ang et al., 2016). ICG and other structurally related fluorophores (e.g., IR800CW) are therefore unsuitable for cell tracking *in-vivo*. More recently, alternative NIR fluorophores have been used to label and track immune cells as they are able to penetrate the cell membrane (e.g. tricarbocyanine *N*-amines), but they rapidly degrade and are unsuitable for long term tracking *in-vivo*.

Photostable, bright and cell-permeable triazole NIR cyanine (TNC) dyes have been rationally designed to overcome the limitations of tricarbocyanine *N*-amines. TNC dyes have successfully tracked inflammatory cells *in-vivo* for up to 7 days without any associated toxicity and are suitable for human T-cell tracking (Mellanby et al., 2018). However, the design and use of TNC dyes to monitor inflammation within the eye has not yet been documented.

In this study, we have explored the use of TNC dyes for direct non-invasive imaging of $CD4^+$T-cells within the eye. Uveitis is a predominantly T-cell mediated event with levels of T-cell recruitment and activation within the eye corresponding with disease severity, therefore, being able to identify the nature and time course of ocular inflammation in real time would revolutionize uveitis management and treatment. Building from our previous studies (Mellanby et al., 2018), we synthesized three TNC dyes based on the *N*-triazole tricarbocyanine core with the inclusion or not of water-solubilizing carboxylic acid groups at different positions of the scaffold. We analysed their optical properties under conventional clinical ICGA imaging and assessed ocular cell toxicity at optically detectable levels and compared the performance of these TNC dyes to the standard ICG in an *ex-vivo* porcine eye model. Excitingly, two of these TNC dyes are ICGA-compatible and suitable for visualising T-cells at non-toxic concentrations supporting their considerable potential as diagnostic markers of ocular inflammation in patients with uveitis.

2. Materials and methods

2.1. Synthesis and characterisation of TNC dyes

We synthesised TNC dyes using previously reported procedures (Mellanby et al., 2018) (Fig. S1A). Briefly, a solution of IR780 or the carboxylic acid analogue (1 eq) in DMF was treated with sodium azide (5 eq) in H_2O and the resulting mixture was stirred at 70 °C for 20 min. Reactions were then cooled down, diluted with CH_2Cl_2 and washed with H_2O. Combined organic layers containing the tricarbocyanine azide intermediate were evaporated and used without further purification. The tricarbocyanine azides were dissolved in CH_2Cl_2 and aliquoted to react with the different alkynes. To each aliquot, we added $CuSO_4$ (2 eq), tris[(1-benzyl-1H-1,2,3-triazol-4-yl)methyl] amine (2 eq) and sodium ascorbate (2 eq) predissolved in DMF: H_2O (1:1), and the alkynes (10 eq). The resulting mixtures were stirred at room temperature for 2 h. The crude reaction mixtures were diluted in CH_2Cl_2, and the organic phases were washed with H_2O. The organic extracts were dried over $MgSO_4$, filtered and evaporated under reduced pressure. The resulting crudes were then purified by semipreparative HPLC to yield the TNC compounds (characterisation including ^1H and ^{13}C NMR spectra in Fig. S2 and Fig. S3). TNC compounds were lyophilised and stored at −20 °C until use. For biological assays, TNC dyes were reconstituted in dimethylsulfoxide (DMSO; Sigma-Aldrich, UK) to 10 mM and stored in light-restricted conditions at −20 °C. ICG (MP Biomedicals, France) was reconstituted in sterile water to 100 mM and further diluted in sterile PBS.

2.2. In-vitro ARPE-19 and human trabecular meshwork cell culture

Human adult retinal pigment epithelial cells (ARPE-19) (CRL-2302; ATTC, Middlesex, UK) were cultured in Dulbecco's modified Eagle's medium: Nutrient Mixture F12 (DMEM-F12) (Gibco) with 10% (v/v) heat inactivated foetal bovine serum (FBS; Gibco) and 1% penicillin-streptomycin (Thermo Fisher Scientific). ARPE-19 cells were passaged at 70% confluence (used between P4–P10). Human trabecular meshwork cells (HTMC; Cell Applications Inc., USA) were cultured in HTMC basal medium with supplements (Cell Applications) as per manufacturer's instructions (used between P4–P6).

2.3. MTT cell viability assay

Cell viability was measured using 3-(4,5-dimethylthiazol-2-yl)-2,5-diphenyltetrazolium bromide (MTT) colorimetric assay kit. ARPE-19 and HTMC were cultured to 70% confluence in 96-well plates, then cultured with treatments for 24 h before performing MTT. A dose range of 100 nM, 1 μM, 10 μM (all in 0.1% DMSO) in PBS were tested for all TNC dyes. ICG was also tested across the same range of 100 nM–10 μM. Cells were also treated with media alone (no treatment) and vehicle controls (0.1% DMSO for the TNC dyes or PBS for ICG). HTMC were plated with HTMC media for 24 h then replaced with 100 μL of phenol red-free DMEM and treatments added for 24 h. In ARPE-19 cells, the cells were plated in DMEM-F12 containing 10% FBS, 1% penicillin-streptomycin. MTT (Vybrant ® MTT-cell Proliferation Assay Kit; Molecular Probes) was performed according to the manufacturer's instructions. The plates were read at 570 nm on a colorimetric plate reader (Infinite 200 Pro; TECAN) and results normalised as % cell viability compared to media only control. Cells were treated in triplicates and experiments were performed on three independent occasions.

2.4. NIR fluorescence spectrophotometry for dye detection

To investigate the quantitative intensity of the TNC dyes we tested a range of concentrations on the NIR spectrum of a fluorescence spectrophotometer. The wavelength absorbance versus concentration was plotted and the strongest linear relationship fitted using best-fit linearity in GraphPad, to interpolate the concentrations of the dyes in the aqueous and vitreous compartments. A range of 0.1 μM, 1 μM, 10 μM (all 0.1% DMSO) and 100 μM (1% DMSO) of TNC dyes were prepared (Fig. S1B). ICG was diluted in PBS.

2.5. SPECTRALIS® detection of dyes

The dyes were also imaged in cuvettes on the ICG angiography (ICGA) setting on the SPECTRALIS® imaging platform (Heidelberg Engineering, Heidelberg) at 10 μM and 100 μM. Cuvettes imaged with a 55° wide field lens on infrared (IR) reflectance setting to visualise the cuvettes and then the ICGA setting with a diode laser at 770 nm excitation and 830 nm emission. The sensitivity was set at a constant level across all groups (107 maximum).

2.6. Intraocular detection of dyes (ex-vivo porcine eyes)

Fresh, adult unscalded porcine eyes were used within 24 h of enucleation (Medical Meat Supplies, Rochdale, UK). Excess extraocular tissue was removed from the eyes and followed by washing with PBS. Dyes were administered to the porcine eyes either via intracameral injections or topical application (Fig. S1C). The eyes were then imaged on the ICGA setting of the SPECTRALIS® and tissue collected for fluorescence analysis. For the intracameral injection of TNC dyes, a self-sealing corneal incision was made using a 15° ophthalmic knife followed by 10 μL injections of 100 μM TNC dyes using a 26-gauge Hamilton syringe. After injection, the eyes were irrigated with PBS to remove any excess dye from the ocular surface. Control groups consisted of 1% DMSO in PBS, PBS or intact eye (n = 3/group). For topical application, filter paper squares (~3 × 3 cm) were impregnated with 60 μL of 100 μM dye and placed centrally on the cornea for 10 min at room temperature. Eyes were then irrigated with PBS to remove excess dye. A vehicle control of 1% DMSO in PBS and a negative control of 60 μL of PBS were used (n = 3/group).

2.7. SPECTRALIS® imaging of porcine eyes

Porcine eyes in 6-well plates (Greiner Bio-One, Austria) were secured for imaging and sealed with the lid opposing but not deforming the cornea to preserve the integrity of the anterior segment. PBS was placed on the cornea to prevent drying and clouding. Porcine eyes were imaged with a 55°wide field lens firstly in IR and then ICGA with a diode laser at 790 nm excitation and 830 nm emission. Sensitivity was set at a constant level across all groups (107 maximum) or set to automatic to detect the optimal image per dye.

2.8. Quantification of SPECTRALIS® ICGA images

Dye intensity from cuvettes and porcine eyes were quantified to measure the integrated density. Image analysis was carried out using Image J software (http://imagej.nih.gov/ij/). For the cuvettes, each image was converted to greyscale and 10 regions of interest (ROI) of equal area were selected per cuvette and raw integrated density measured. To quantify the intensity of dye fluorescence in the porcine eyes, images were converted to greyscale, the limbus measured on the IR and saved as a ROI. This ROI was imported onto the ICGA image, and the integrated density and area recorded and calculated as integrated density per mm^2.

2.9. Detection of dyes in aqueous and vitreous humour

Immediately following ICGA imaging of the porcine eyes, aqueous and vitreous humour was collected, and fluorescent intensity quantified using a fluorescent plate reader. The aqueous humour (~200 μL) was collected using a 21-gauge needle (Henke Sass Wolf, Germany) and vitreous removed for storage at −20 °C in the dark. Samples were thawed on ice and 30 μL from each sample were then measured in triplicates at 770 nm excitation and 830 nm emission on a Spark® Multimode Microplate reader (TECAN). The concentration of dyes in graphs (Fig. 1) were used to interpolate the concentration of dyes in the aqueous and vitreous from the relative fluorescent intensity.

2.10. Detection of $CD4^+$T-cells labelled with TNC dyes in ex-vivo porcine eyes

Human peripheral blood $CD4^+$T-cells (HPBT; 5×10^6 cells; Cell Applications Inc. 6902-50a) were cultured with human blood medium (Cell Applications Inc., 615–250) for 3 days at 37 °C and 5% CO_2. $CD4^+$T-cells (~5×10^5 cells per group) were incubated with 10 μM of TNC-1, TNC-2, TNC-3, ICG or vehicle (DMSO for TNC or PBS for ICG) in PBS for 5 min at 37 °C before washing in PBS, centrifugation at 400*g* for 5 min and re-suspension in 40 μL of human blood medium. Approximately 10^5 x$CD4^+$T-cells were pipetted into 300 μL of PBS in cuvettes and 10 μL of the solution intracamerally injected (~10^5 cells) into porcine eyes. Cuvettes and porcine eyes were then imaged using SPECTRALIS® ICGA.

2.11. Mechanism of TNC uptake into CD4+T-cells

Leukocyte cones (NHS-BTS; all samples were obtained with informed consent and with approval from the appropriate Research Ethics Committee (REC Reference 20/WA/0216) derived from healthy donors (n = 3 individual donors with cells from each donor assessed in triplicate for all conditions) were used to prepare peripheral blood mononuclear cells

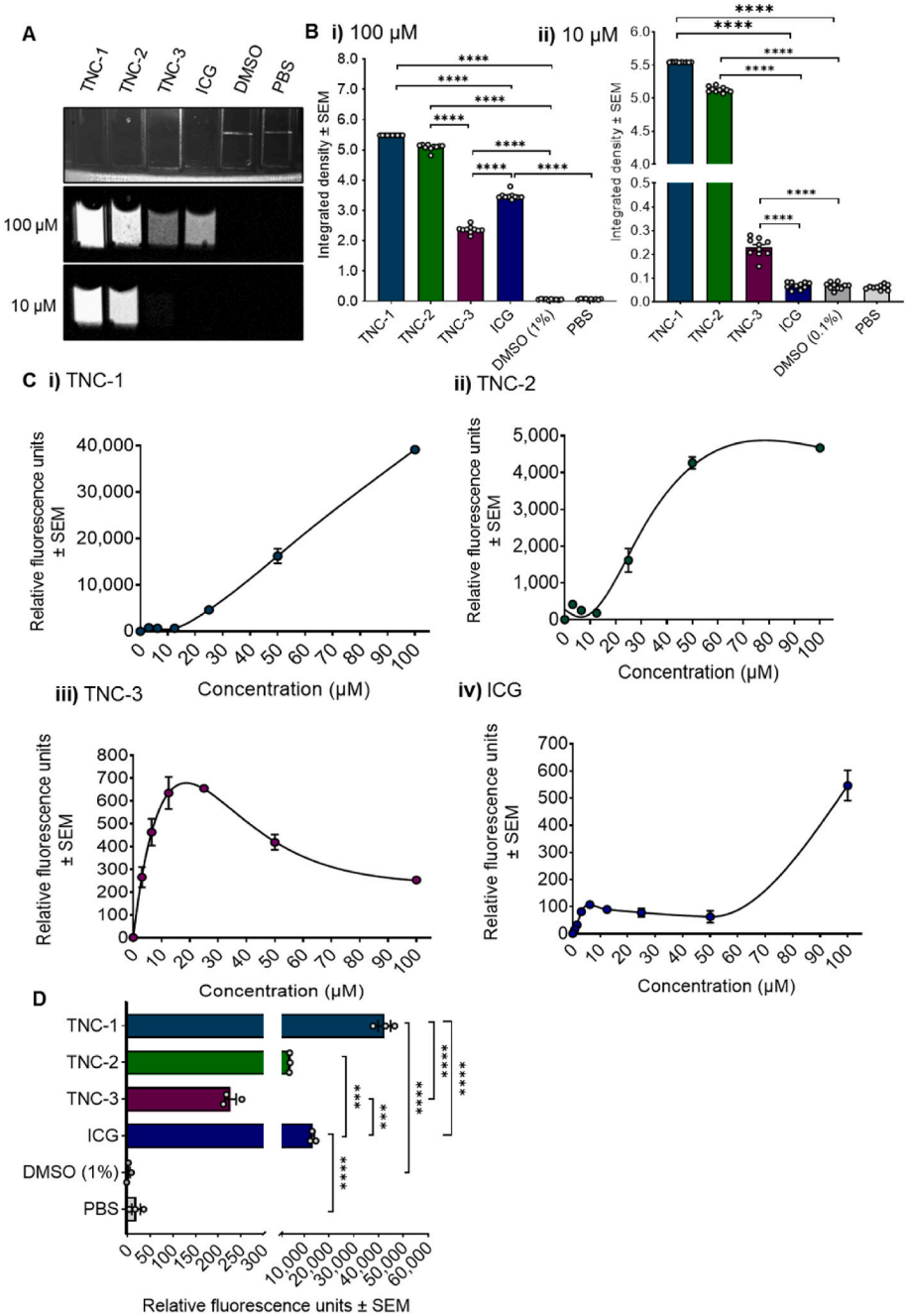

Fig. 1. Detection and quantification of TNC dyes **A)** Detection of TNC dyes, ICG and vehicle controls using SPECTRALIS® ICGA. **B)** Quantification of the integrated density of the dyes at **i)** 100 μM and **ii)** 10 μM using SPECTRALIS® ICGA. **C)** Quantification of TNC dyes and ICG on the fluorescence spectrophotometer (excitation 780 nm, emission 820 nm) for i) TNC-1, ii) TNC-2, iii) TNC-3 and iv) ICG. **D)** Relative fluorescence signals of TNC dyes, ICG and vehicle controls at 100 μM ***$P < 0.001$, ****$P < 0.0001$. Values represent mean ± SEM.

(PBMCs) using SepMate density gradient centrifugation (StemCell Technologies, 85450) with Ficoll-Paque PLUS (GE Healthcare; 11778538). $CD4^+$T-cells were enriched using a human $CD4^+$ T-cell isolation kit (StemCell Technologies; 17952). Isolated cells were rested in 96-well glass bottomed imaging plates (Corning; 4580) in RPMI (Sigma; R8758) with 10% FBS (Sigma; F9665) and 1% penicillin-streptomycin (Gibco; 15070) for 2 h (37 °C and 5% CO_2) before incubation in the absence (DMSO vehicle control) or presence of dynole 34–2 (50 μM; Tocris; 4222) for 30 min at 37 °C, followed by incubation with TNC-1 (10 μM) or vehicle (0.1% DMSO) or TNC-2 (100 μM) or vehicle (1% DMSO) containing Hoechst 33342 nuclear stain (Thermofisher; 62249) for 15 min at 37 °C. Live cell imaging was performed using high-content confocal imaging (Yokogawa CQ1 imaging platform; ×40 objective lens, imaging 3 fields of view/well). Dye uptake into cells was quantified as total intensity per cell, using CQ1 image analysis software (version 1.02.02.00).

2.12. Statistics

Statistical analyses were performed using GraphPad Prism8 software. Data were tested for normality using the Shapiro-Wilk test and normally distributed data were analysed using one-way ANOVA and post-hoc Tukey tests with P values corrected for multiple comparisons. Values represent mean ± standard error of the mean (SEM).

3. Results and discussion

3.1. Detection of TNC dyes using ICGA imaging

We examined a subset of tricarbocyanine dyes (Fig. S1), TNC dyes, with a clinical imaging system and observed stronger signals compared to ICG, thus enabling visualisation at lower concentrations. TNC-1 displayed the strongest intensity, followed by TNC-2, ICG and TNC-3 on

ICGA (Fig. 1A). At 100 μM, TNC-1, TNC-2 and TNC-3 reported a significant increase in fluorescent signal compared to DMSO vehicle (5.48 RID ± 0.0003; $P < 0.0001$, 5.09 RID ± 0.032; $P < 0.0001$ and 2.37 RID ± 0.037; $P < 0.0001$, respectively) and ICG was significantly brighter compared to PBS vehicle (3.48 RID ± 0.037; $P < 0.0001$) (Fig. 1B). Moreover, TNC-1 and TNC-2 were significantly brighter than ICG ($P < 0.0001$ and $P < 0.001$), but TNC-3 reported a weaker signal than ICG ($P < 0.0001$). At 10 μM, only TNC-1 and TNC-2 were visible, with minimal detectable signal from TNC-3 and no detectable ICG signal. TNC fluorescence was quantified and its integrated density was plotted (Fig. 1B). At 10 μM, all TNC dyes were significantly brighter than DMSO and ICG groups, whilst ICG produced an equivalent signal compared to its PBS vehicle.

TNC dyes incorporate chemical groups (e.g., *N*-triazoles) that can overcome photodegradation and aggregation issues associated with other NIR tricarbocyanine dyes such as ICG. Furthermore, we synthesised derivatives including carboxylic acids at different positions of the tricarbocyanine core to enhance water suitability and enable future bioconjugation studies.

3.2. Quantification of dyes and interpolation of concentrations on a fluorescent plate reader

TNC dyes were measured at a range of concentrations (10–100 μM)

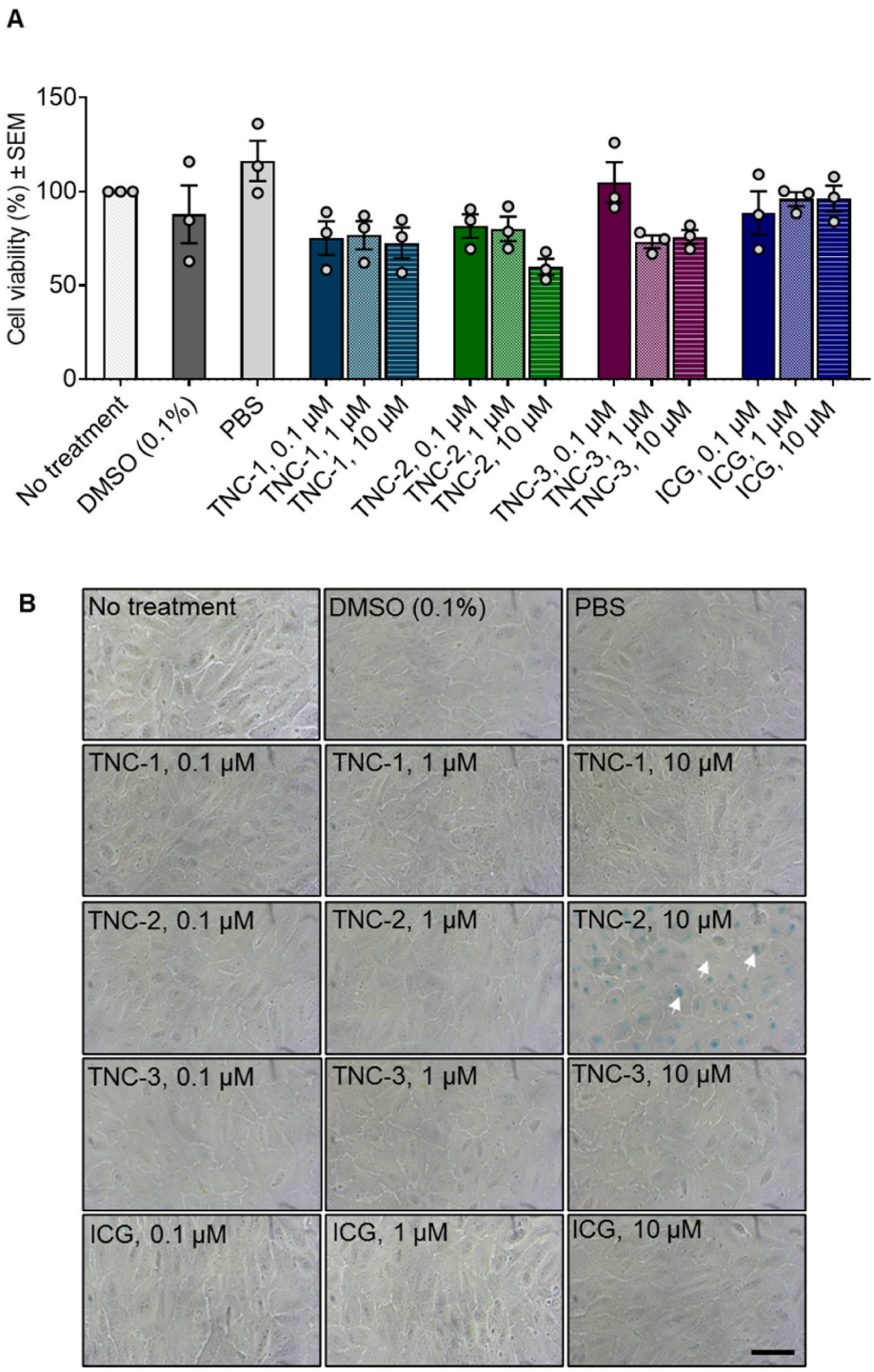

Fig. 2. TNC dye effects on ARPE-19 cell viability at 0.1 μM, 1 μM and 10 μM. **A)** Quantification of mean % cell viability after 24 h incubation with TNC dyes, ICG and their respective vehicle controls. One-way ANOVA's with Tukey's post-hoc multiple comparison test was performed for comparison of each dye to their respective vehicle groups. **B)** Representative bright-field microscopy images of ARPE-19 cells after 24 h incubation with treatments. White arrows indicate dye in cell nuclei after TNC-2 dye treatment. Treatments were performed in triplicate and on three independent occasions. Values represent mean ± SEM. Scale bar = 20 μm.

for which their relative fluorescent units (RFU) were determined. At 100 μM and 10 μM, TNC-1 and TNC-2 are brightest, then ICG then TNC (Fig. 1A&B). TNC-1 showed increased RFU as the concentration increased (Fig. 1Ci) and displayed the brightest signals of the dyes, with ~40,000 RFU at 100 μM concentration. The relative fluorescent intensity of TNC-2 was 10-fold lower than TNC-1 (Fig. 1Cii), with ~4000 RFU at 100 μM. TNC-2 dye showed features of quenching with the emission reaching a plateau at 50–100 μM. TNC-3 had the weakest emission of all TNC dyes (Fig. 1Ciii), with approximately 10-fold lower values than TNC-2 and 100-fold lower RFU than TNC-1. The RFU values of ICG did not show a correlation with increased concentration and reached a plateau up to 50 μM, with an increased RFU at 100 μM up to 500 RFU (Fig. 1Civ). In order for the concentration of dyes to be determined in further experiments, lines of best fit were measured at 100 μM, 50 μM, 25 μM, 12.5 μM, 7.25 μM and 3.125 μM for each dye and later used to interpolate the concentration of dyes from the relative fluorescent units in the aqueous and vitreous samples taken from porcine eyes. On the fluorescent plate reader (Fig. 1D), TNC-1 is brightest followed by ICG and TNC-2, with TNC-3 being the least fluorescent.

3.3. TNC dyes do not affect T-cell viability in ARPE-19 cells or HTMC at working concentrations for ICGA imaging

To determine if TNC dyes would be toxic to cells in the posterior segment of the eye, we performed MTT assays on ARPE-19 cells,

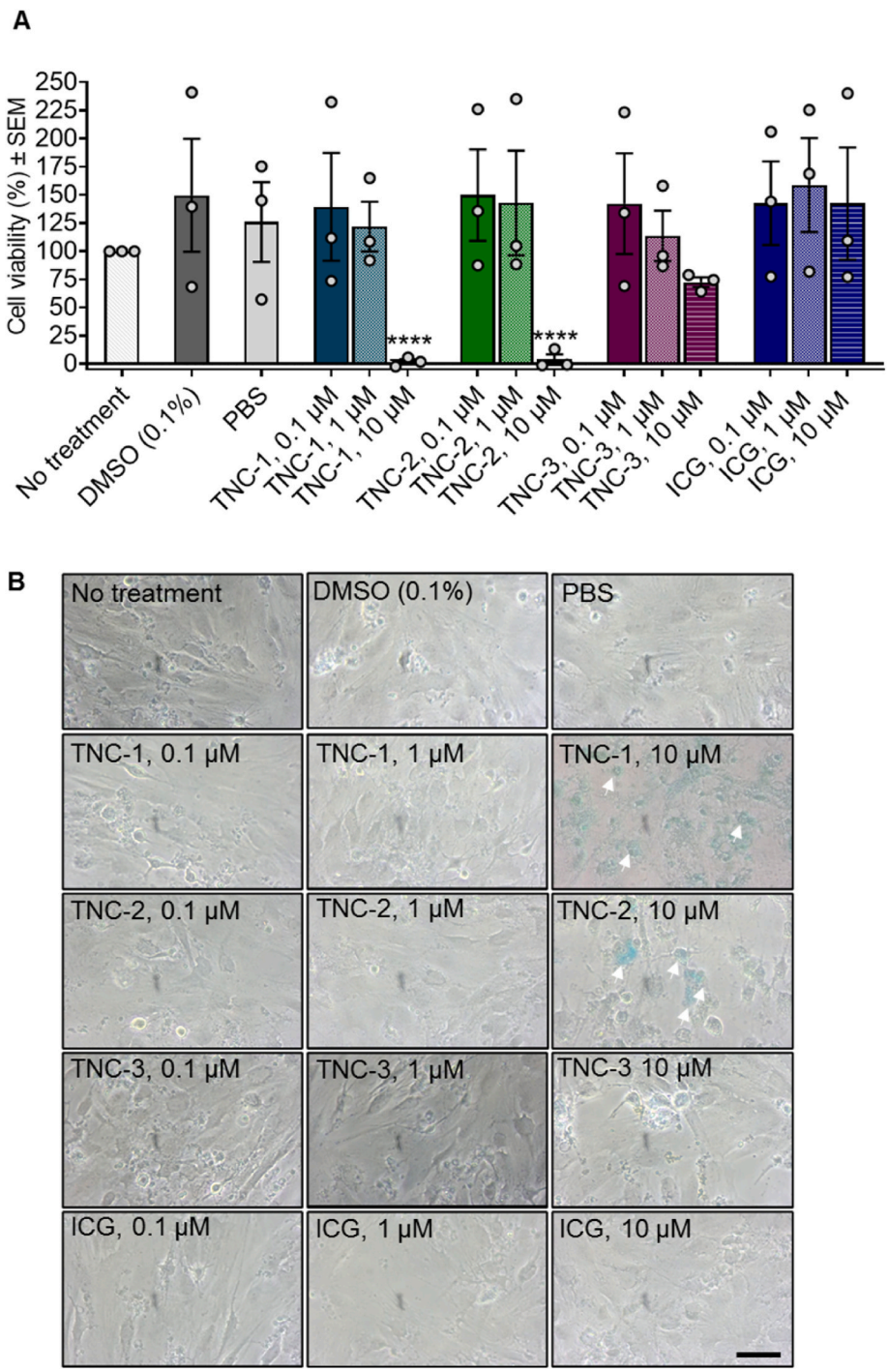

Fig. 3. TNC dyes effects on HTMC viability at 0.1 μM, 1 μM and 10 μM. **A)** Quantification of mean % cell viability after 24 h incubation with TNC dyes, ICG or their vehicle controls. One-way ANOVA's with Tukey's post-hoc multiple comparison test was performed for comparison of each dye to their respective vehicle groups. ****$P < 0.0001$. **B)** Representative bright-field microscopy images of HTMC after 24 h incubation with treatments. Treatments were performed in triplicate and in three independent experiments. Values represent mean ± SEM. Scale bar = 20 μM.

incubated with a range of concentrations for 24 h (Fig. 2). There were no significant differences in cell viability at 10 μM, 1 μM and 100 nM for TNC-1, TNC-2, TNC-3 and ICG compared to 'no treatment', 0.1% DMSO (TNC vehicle) or PBS (ICG vehicle); therefore, we concluded that dyes <10 μM would not affect the viability of ARPE-19 cells. Interestingly, there were nuclear aggregates observed in ARPE-19 after incubation with 10 μM of TNC-2 (Fig. 2B, white arrows). Cyanine dyes have high affinity for proteins and can aggregate in water solutions, reducing their activity (Kraft and Ho, 2014). Cyanine aggregates could potentially alter T-cell behaviour and the influence of off target effects on cell function with the eye, and therefore would need to further investigated in mouse models.

Some cyanine dyes are unstable in aqueous conditions, in particular when exposed to light. Upon irradiation, ICG can produce singlet oxygen and induce apoptosis and necrosis (Shirata et al., 2017). For instance, Narayan et al. detected high levels of thymidine incorporation when ARPE-19 were treated with ICG (Yam et al., 2003; Narayanan et al., 2005). DMSO can display toxicity to ocular cells at concentrations >0.5%, as it increases the cell membrane permeability (Notman et al., 2006; de Ménorval et al., 2012; Galvao et al., 2014); however, in our current study, cells treated with DMSO did not show a significant effect of cellular viability compared to cells incubated with media only.

We also observed that TNC dyes did not affect the viability of HTMC at 0.1 μM and 1.0 μM when compared to no treatment, DMSO or PBS *in-vitro* (Fig. 3A). This experiment was performed to determine and toxicity in HTMC located in the anterior segment of the eye. Concentrations of TNC dyes at 10 μM reduced HTMC viability after TNC-1 (1.812 ± 2.301%; $P = 0.0287$) and TNC-2 (3.856 ± 4.724%; $P = 0.0316$) when

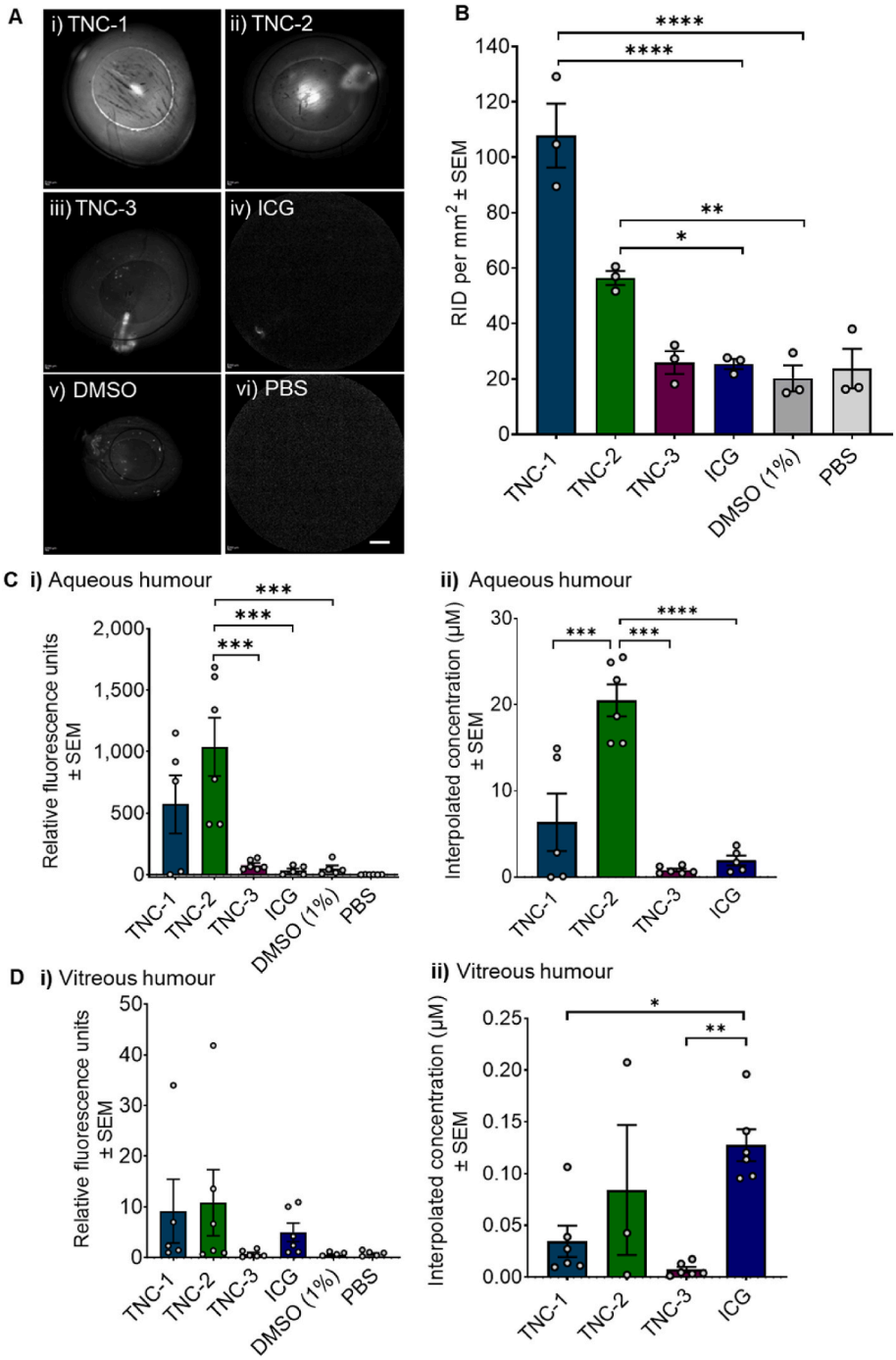

Fig. 4. Visualisation and quantification after TNC and ICG dyes injected into the aqueous humour of porcine eyes. **A)** Representative ICGA images of porcine eyes following injection of **(i-vi)** 100 μM TNC-1,2,3, ICG, DMSO or PBS into the anterior chamber. N = 3 eyes/group. **B)** Quantification of relative integrated density (RID) for each treatment group. **C)** Quantification of the aqueous humour showing **i)** relative fluorescent units and **ii)** corresponding concentrations interpolated from associated standard curves. **D)** Quantification of the vitreous humour showing **i)** relative fluorescent units and **ii)** corresponding concentrations interpolated from associated standard curves. $^{*}P < 0.05$, $^{**}P < 0.01$, $^{***}P < 0.001$, $^{****}P < 0.0001$. One-way ANOVA with Tukey's post-hoc multiple comparison test. Values represent mean ± SEM. Scale bar = 1 mm.

compared to DMSO, but there was only a slight reduction in viability treated with TNC-3, which was not significantly lower (72.62 ± 4.345%; $P = 0.4922$) compared to DMSO. There was no loss of cell viability in ICG dye treated cells compared to PBS vehicle at any concentrations (ANOVA, $P = 0.3218$). However, 10 μM concentrations administered into the eye (rather then placed directly onto cells) would be further diluted when placed into the eye, for example, the final concentration of 10 μL of 100 μM TNC dyes injected into the anterior chamber (~300 μL) is approximately 3 μM inside the eye, and therefore would be within the range of non-toxic concentrations shown in these *in-vitro* experiments. Dye aggregation also occurred in the HTMC nucleus after 24 h incubation with 10 μM TNC-1 and TNC-2 (Fig. 3B, white arrows).

It was interesting to note the differences in toxicity between the two cell types. ARPE-19 medium contains protein-rich FBS and could have provided an antioxidant effect and hence lower toxicity at 10 μM compared to HTMC. Finally, the conditions of *in-vitro* assays do not replicate the pharmacokinetics and out flow in the eye *in-vivo*. The eye has multiple static and dynamic barriers which will affect the bioavailability of compounds (Cholkar et al., 2013). For example, in the anterior chamber, the aqueous humour turnover and outflow, aqueous humour volume, melanin drug binding and ocular enzymes can all affect the drug concentration, degradation and duration of exposure of the ocular cells. The ocular cells were exposed to these concentrations for 24 h *in-vitro* conditions, whereas *in-vivo* the aqueous humour turnover is estimated to be between 1.0% and 1.5% of the anterior chamber volume per minute (Goel et al., 2010), demonstrating high turnover and a reduced risk of toxicity due to high clearance rate following imaging.

3.4. TNC dyes injected into the aqueous humour detected on ICGA

In this present study, we first determined if we could detect TNC dyes when injected into the anterior chamber in a porcine *ex-vivo* model which is a surrogate in size and anatomy for a human eye. We observed clear detection of TNC dyes when injected with 10 μL of 100 μM into the anterior segment of the porcine eyes, and they were brighter than ICG (Fig. 4). We could also observe signals in porcine eyes when dyes were diluted to 100 nM in the aqueous humour, highlighting the sensitivity of the TNC dyes for ICGA imaging. We showed that TNC-1, TNC-2 and TNC-3 can be detected on ICGA (Fig. 4A), with the signal of ICG being the weakest and comparable to DMSO (which may also possess some intrinsic fluorescence). We quantified the RID (Fig. 4B) and demonstrated that TNC-1 and TNC-2 were significantly brighter than DMSO (107.8 ± 11.54; $P < 0.0001$ and 56.42 ± 2.56; $P = 0.0059$, respectively) and brighter than porcine eyes injected with ICG ($P < 0.0001$ and $P = 0.0165$). TNC-3 and ICG were not significantly brighter than their DMSO or PBS vehicle controls, and TNC-3 was not significantly brighter than ICG. Additionally, studies have found that <5% of topically applied molecules can reach deep areas of ocular tissues (Patel et al., 2013); therefore, the dyes that are applied in the eye are likely to be cleared relatively quickly after imaging and are unlikely to reach the posterior segment in high concentrations.

TNC-1 and TNC-2 (both including one carboxylic acid group) showed increased solubility in aqueous solutions (e.g., aqueous humour) and stronger signals than TNC-3, which does not have a carboxylic acid group. We confirmed this observation in porcine eyes, where we detected aggregates of TNC-3 (but not for TNC-1 and TNC-2) in the anterior segment. We confirmed this observation in porcine eyes, where we detected aggregates of TNC-3 (but not for TNC-1 and TNC-2) in the anterior segment.

3.5. Quantification of TNC dyes in the aqueous and vitreous

To determine if we could quantify the levels of TNC dyes, we collected aqueous from the porcine and measured the RFU on a fluorescent plate reader (Fig. 4C and D). In the aqueous humour TNC-2 produced a significantly greater signal (1038 RFU ± 237.6) compared to DMSO vehicle (49.12 ± 24.48; $P = 0.0001$), ICG (33.40 ± 16.35; $P = 0.0001$) and TNC-3 (78.38 ± 16.13; $P = 0.0001$) (Fig. 4C). Interestingly, TNC-1 and TNC-3 were not significantly brighter than the DMSO vehicle. Additionally, ICG was not significantly brighter than its PBS vehicle (0.18 RFU ± 0.41). In the vitreous, TNC-2 was detected in higher levels compared to TNC-1 and TNC-3, and was similar to ICG levels.

Although TNC-1 was superior *in-vitro*, when placed into the eye, TNC-2 was detected in higher levels. TNC-3 was weak across both *in-vitro* and *ex-vivo* assays suggesting that the dosing required for TNC-3 would be far higher than TNC-1 or TNC-2.

3.6. Visualisation and quantification of TNC dyes after topical application

The administration route of TNC dyes is important to ensure optimal acceptance amongst patients. Intraocular injections are invasive, not pleasant for patients and can have side effects including endophthalmitis, retinal detachment, elevated intraocular pressure and subconjunctival haemorrhage, hence topical application may be preferred but poses issues with bioavailability.

We visualised the TNC dyes on ICGA after topical application to determine if topical administration of the dyes could penetrate the cornea and enter into the aqueous humour (Fig. 5A). TNC-1, TNC-2 and TNC-3 could be readily visualised, with TNC-1 being the brightest dye (83.54 RID ± 6.89). TNC-1 displayed significantly brighter signals compared to TNC-2 (38.79 RID ± 6.975; $P = 0.0024$) but was not significant brighter when compared to TNC-3 (55.39 ± 11.15 RID; $P = 0.0589$). ICG demonstrated a significantly weaker signal (18.82 RID ± 2.35) compared to both TNC-1 and TNC-3 ($P < 0.001$ and $P = 0.0114$, respectively), although no significance was recorded when compared to TNC-2 ($P = 0.2601$). All TNC dyes were significantly brighter than DMSO (3.20 RID ± 0.42; $P < 0.001$, $P = 0.0138$ and $P = 0.0006$).

Fluorescent signals outside of the limbus were observed, suggesting that the dye could have remained on the surface of the eye despite extensive PBS washes. To determine if the dyes had penetrated the eye, we also collected aqueous and vitreous humour for quantification (Fig. 5Ci). TNC-1 displayed the brightest signal (20.13 RFU ± 12.26) followed by TNC-2 (19.24 RFU ± 3.79), with TNC-3 and ICG displaying weak signals in the aqueous. Although ICG produced a very weak fluorescent signal in the raw RFU values, it still demonstrated the highest interpolated concentration in the aqueous (0.106 ± 0.005 μM). This was significantly greater than TNC-3 ($P = 0.44$, Fig. 5Cii). TNC-1 and TNC-2 dyes presented with the highest interpolated concentrations (0.075 ± 0.022 μM and 0.066 ± 0.036 μM), whilst the concentration of TNC-3 was negligible (0.0071 ± 0.0019 μM). In the vitreous, none of the TNC dyes were significantly brighter than DMSO or ICG, and ICG was not significantly brighter than PBS (Fig. 5D). Similar to the aqueous, ICG presented the highest interpolated concentration in the vitreous (0.074 ± 0.014 μM, Fig. 5Dii), and this was significantly higher than TNC-3 and TNC-2 ($P = 0.0184$ and $P = 0.0199$, respectively).

We did detect signals outside of the limbus on ICGA scans, so could not determine if the dyes penetrated the aqueous humour or if they were binding to the cornea. This was mitigated by measuring levels directly from aqueous humour. We found high fluorescence levels in aqueous humour samples, suggesting that TNC dyes can enter the anterior chamber. Because TNC dyes are amphiphilic, they may possess optimal features for penetrating the cornea as the cornea contains both hydrophilic and hydrophobic barriers (Cholkar et al., 2013).

We also observed that the dyes were not distributed homogeneously throughout the eye, which suggests that they may accumulate or cluster in different segments, such as the lens and iris. The lens capsule is rich in hydrophobic collagen type IV and sulphated glycosaminoglycan and the iris contains high levels of melanin, which has been shown to bind several drugs including ephedrine (Danysh and Duncan, 2009; Agrahari et al., 2016). ICG has high affinity for extracellular matrix components (e.g., collagen) and has been used in the past during ophthalmic surgery

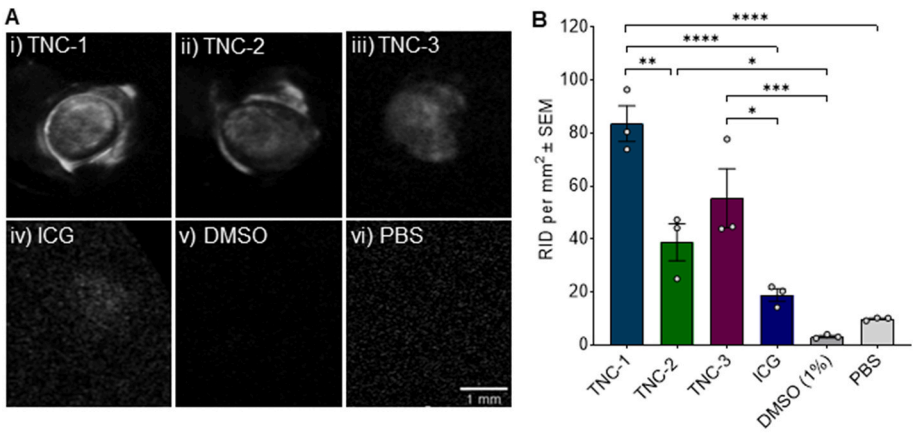

Fig. 5. Visualisation and quantification after TNC and ICG dyes were applied by topical application in porcine eyes. **A)** Representative ICGA images following topical application of TNC dyes, ICG, DMSO and PBS. **B)** Quantification of relative integrated density (RID) for each treatment group (n = 3 eyes/group). **C)** Quantification of aqueous humour showing **i)** relative fluorescent units and **ii)** corresponding concentrations interpolated from associated standard curves. **D)** Quantification of the vitreous humour fluorescence showing **i)** relative fluorescent units and **ii)** corresponding concentrations interpolated from associated standard curves Fig.1C. *$P < 0.05$, **$P < 0.01$, ***$P < 0.001$, ****$P < 0.0001$. One-way ANOVA with Tukey's post-hoc multiple comparison test. Values represent mean ± SEM. Scale bar = 1 mm.

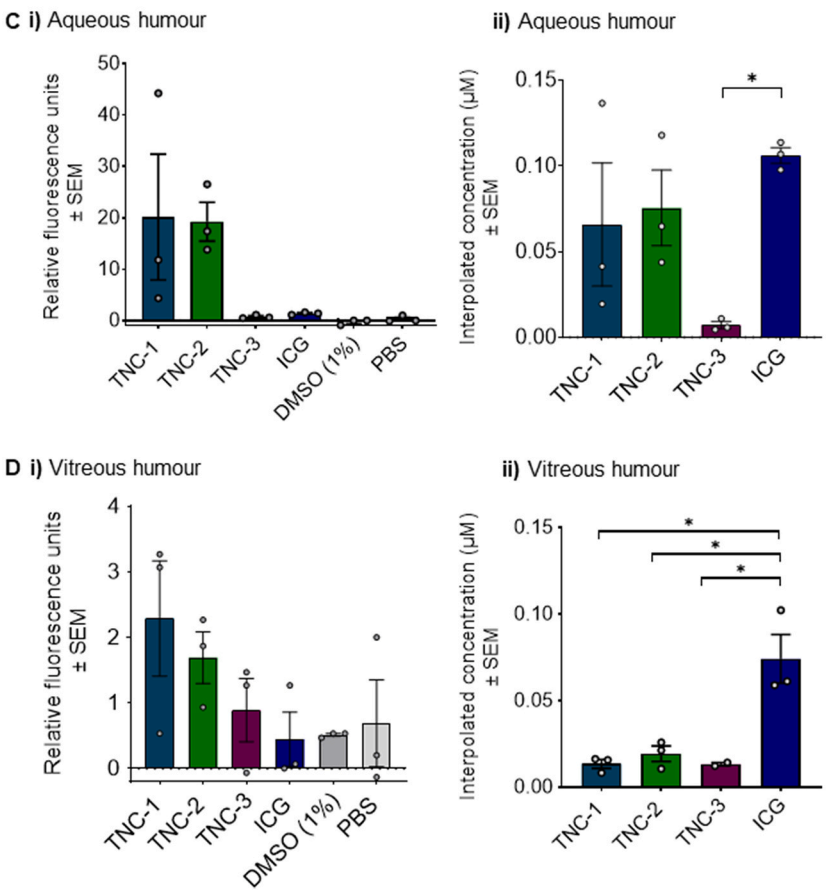

to stain the transparent, acellular internal limiting membrane at the interface between the vitreous and retina (Mavrofrides et al., 2006; Noguchi et al., 2018). We have shown that very small amounts of TNC dyes relocate in the vitreous, which suggests that they can penetrate both the anterior and posterior portion of the eye but at very small amounts and thus would likely require tweaks to the structure or an additional agent for optimal delivery to some specific regions of the eye (Pescina et al., 2018).

3.7. TNC is actively taken up into CD4$^+$T-cells and can be imaged on ICGA

We examined if TNC labelled CD4$^+$T-cells could be detected on ICGA. We incubated cells with all dyes -including ICG-at a concentration of 10 μM and the resulting cell suspensions (approximately 10^5xCD4$^+$T-cells) were diluted with 300 μL of PBS and imaged. CD4+T-cell suspensions were first imaged in cuvettes (Fig. 6A) and quantified (Fig. 6B), with all TNC dyes significantly brighter when compared to their vehicle controls and ICG. TNC-2 was the brightest dye (6.07 RID ± 0.21; $P < 0.0001$), followed by TNC-3 (3.29 RID ± 0.073; $P < 0.0001$) and TNC-1 (2.11 RID ± 0.062; $P < 0.0001$). ICG showed weak signals but significantly brighter than PBS (1.39 RID ± 0.039; $P < 0.0001$). Next, we used the same procedure to label CD4$^+$T-cells and inject them intracamerally into porcine eyes. All TNC dyes were detectable and brighter than ICG (Fig. 6C). These were quantified (Fig. 6D), with TNC-2 displaying the brightest signal (84.72 RID ± 16.13), followed by TNC-1 (71.92 RID ± 9.39), with both dyes significantly brighter than DMSO ($P = 0.0128$ and $P = 0.0496$, respectively). ICG was negligibly brighter than its PBS vehicle. Furthermore, we determined if TNC-1 and TNC-2 dyes were actively taken up into CD4$^+$T-cells. To study the mechanism of uptake, CD4$^+$T-cells were incubated with the dynamin inhibitor, dynole 34–2 (or vehicle control), before incubation with TNC-1 (10 μM).

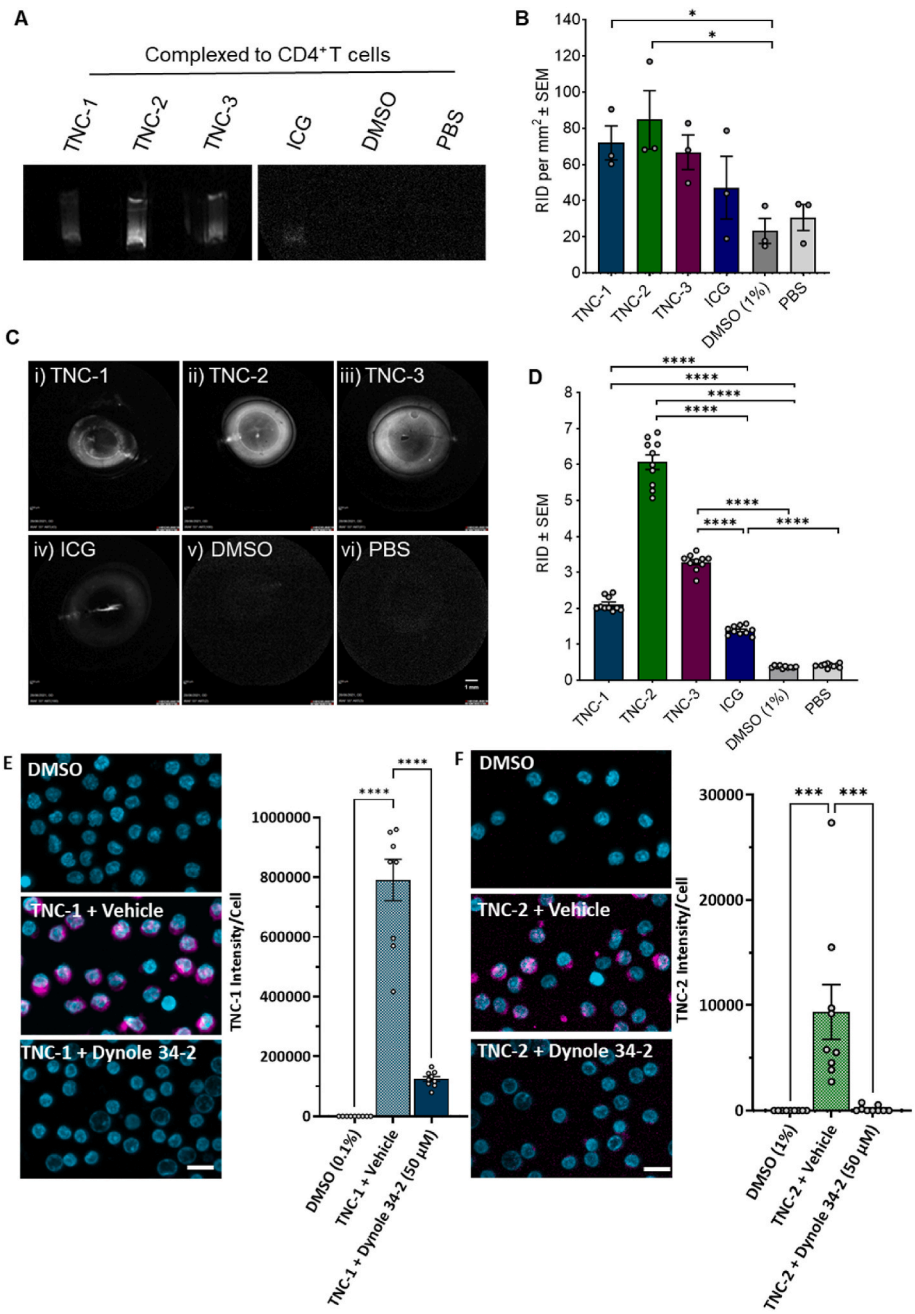

Fig. 6. Labelling and post transfer detection of primary CD4$^+$T-cells and impact of endocytosis inhibitors on TNC labelling of primary CD4$^+$T-cells. **A)** Representative ICGA image (n = 3 eyes/group). **B)** Quantification of the integrated density. **C)** Representative ICGA images porcine eyes receiving 10 μL 10^5 cells CD4$^+$T-cells treated with 100 μM of TNC-1,2,3, ICG, DMSO or PBS (n = 3 eyes/group) **D)** Quantification of the relative integrated density (RID) of the porcine eyes. Representative images and quantification (intensity/cell) of human CD4$^+$T-cells labelled in the absence (DMSO) or presence of **E)** 10 μM TNC-1 or **F)** 100 μM TNC-2, following pre-incubation in the absence or presence dynole 34–2 (50 μM). One-way ANOVA with Tukey's post-hoc multiple comparison test. *$P < 0.05$, ***$P < 0.001$, ****$P < 0.0001$. Values represent mean ± SEM. Scale bar for C = 1 mm; E & F = 10 μm.

Dynole inhibits dynamin and dynamin is a GTPase which enables membrane fission during clathrin-medicated endocytosis (Robertson et al., 2014). Human CD4$^+$T-cells demonstrated higher fluorescence intensity/cell with TNC-1 compared to TNC-2 at 100 μM (Fig. 6E and F). T-cell labelling by both TNC-1 and TNC-2 was prevented by dynole 34–2 indicating the dye uptake is an active process, most likely via dynamin-dependent endocytosis/pinocytosis.

There is proof of concept in mouse that infiltrating cells can be actively imaged with ICG (Sim et al., 2015) however, imaging immune cells in deeper retinal layers or the heavily pigmented choroid will necessitate the use of fluorescent labels. Previous studies have demonstrated that ICG could label infiltrating leukocytes in a laser-induced CNV mouse model of age-related macular degeneration (AMD) after depot administration (Sim et al., 2015), but intravenous ICG was insufficient to detect immune cell labelling in the human eye (Bell et al., 2020).

4. Conclusions

Our results demonstrate that TNC dyes are superior to ICG for visualisation of CD4$^+$T-cells in an *ex-vivo* porcine eye model, which has similar anatomical properties and size to a human eye and can be visualised using standard clinical equipment. We also provide evidence that TNC dyes are not toxic to ocular cells at suitable concentrations and are actively taken into CD4$^+$T-cells allowing visualisation.

There are currently no robust methods for visualising and tracking immune cells in the human eye. Visualisation of posterior inflammation in retinal inflammatory disease such as posterior uveitis and AMD would be of great clinical value. Recent studies have identified label-free visualisation of a subset of immune cells is possible in the mouse using adaptive optics (Joseph et al., 2020), or in man though restricted to the inner retina alone (Hammer et al., 2020; Migacz et al., 2022) but these label-free approaches cannot reach cells in the choroid so alternative

approaches, such as the TNC dye labelling, may help in this regard. Our TNC dyes offer advantages compared to other inflammatory detection methods as TNC dyes are brighter than the gold standard ICG and can be readily conjugated to different biomolecules or cells for targeted imaging. The high brightness of TNC dyes (in particular TNC-1) enables the use of low concentrations reducing any potential side effects or cytotoxicity. The synthetic approach to our TNC dyes allows for reasonable yields and high purities that will benefit their clinical use.

This proof-of-concept work provides the basis for exploring the potential application of our TNC-labelling approach to live immunophenotyping other serious forms of inflammatory eye disease, such as keratitis, scleritis and other sight-threatening diseases of the ocular surface. However, our studies are limited to *in-vitro* and *ex-vivo* modelling and therefore our ability to track endogenous T-cells within the mouse or human eye has not yet been demonstrated. Given that we have shown that the same TNC dyes can detect endogenous T-cell activation systemically, and that we can successfully detect the dyes within eyes, we are confident that endogenous ocular T-cells will be detected. Future experiments should seek to use the TNC dyes in a mouse model of experimental uveitis (Agarwal et al., 2012) and this will help progress towards clinical utility to help diagnose, manage and treat leading causes of blindness.

Author contributions

Chloe N Thomas: Conceptualization, Methodology, Validation, Formal Analysis, Investigation, Data Curation, Writing – Original Draft, Writing – Review & Editing, Visualisation; **Nada Alfahad:** Methodology, Validation, Formal Analysis, Investigation, Writing – Original Draft; **Nicholas Capewell:** Investigation, Resources, Writing – Review & Editing; **Jamie Cowley:** Formal Analysis, Investigation, Writing – Review & Editing; **Eleanor Hickman:** Formal Analysis, Investigation, Writing – Review & Editing **Antonio Fernandez:** Resources, Writing – Review & Editing; **Neale Harrison:** Data curation; **Omar S Qureshi:** Data curation, analysis, Writing – Editing; **Naomi Bennett:** Investigation, Resources; **Nicholas M Barnes:** Methodology, Writing – Review & Editing**; Andrew D Dick:** Writing – Review & Editing **Colin Chu:** Writing – Review & Editing **Xiaoxuan Liu:** Conceptualization, Methodology, Writing – Review & Editing **Alastair K Denniston:** Conceptualization, Methodology, Validation, Writing – Review & Editing **Marc Vendrell:** Conceptualization, Methodology, Formal Analysis, Writing – Review & Editing, Visualisation **Lisa J Hill:** Conceptualization, Methodology, Validation, Formal Analysis, Investigation, Writing – Review & Editing, Visualisation, Supervision, Project administration, Funding acquisition. All authors approved the final manuscript submission.

Declaration of competing interest

The authors declare that they have no known competing financial interests or personal relationships that could have appeared to influence the work reported in this paper.

Acknowledgments

Chloe N Thomas and Lisa J Hill acknowledge funding from a Research Development Fund from the College of Medical and Dental Sciences at University of Birmingham. Antonio Fernandez acknowledges funding from Fundación Seneca for a Saavedra Fajardo Grant (21124/SF/19). Marc Vendrell acknowledges funding from an ERC Consolidator Grant (DYNAFLUORS, 771443).

Appendix ASupplementary data

Supplementary data to this article can be found online at https://doi.org/10.1016/j.bios.2022.114623.

References

Agarwal, R.K., et al., 2012. Methods Mol. Biol. 900, 443–469.
Agrahari, V., et al., 2016. Drug Deliv. Transl. Res. 6 (6), 735–754.
Alander, J.T., et al., 2012. Int. J. Biomed. Imag. 2012, 940585.
Ang, M., et al., 2016. Br. J. Ophthalmol. 100 (11), 1557–1563.
Awad, D., et al., 2018. Eur. J. Ophthalmol. 28 (4), 433–440.
Bell, O.H., et al., 2020. PLoS One 15 (2), e0226311.
Benson, S., et al., 2019. Angew Chem. Int. Ed. Engl. 58 (21), 6911–6915.
Cao, C., et al., 2019. ACS Appl. Mater. Interfaces 11 (17), 15298–15305.
Cheng, Z., et al., 2020. Nat. Rev. Chem 4 (6), 275–290.
Cholkar, K., et al., 2013. Eye: Anatomy, Physiology and Barriers to Drug Delivery. Elsevier, pp. 1–36.
Curtin, N., et al., 2021. Int. J. Med. Sci. 18 (7), 1541–1553.
Danysh, B.P., Duncan, M.K., 2009. Exp. Eye Res. 88 (2), 151–164.
de Boer, J., et al., 2003. Br. J. Ophthalmol. 87 (7), 879–884.
de Ménorval, M.A., et al., 2012. PLoS One 7 (7), e41733.
Fernandez, A., et al., 2017. ACS Cent. Sci. 3 (9), 995–1005.
Galvao, J., et al., 2014. Faseb. J. 28 (3), 1317–1330.
Goel, M., et al., 2010. Open Ophthalmol. J. 4, 52–59.
Hammer, D.X., et al., 2020. Proc. Natl. Acad. Sci. USA 117 (48), 30661–30669.
Han, X., et al., 2017. Adv. Funct. Mater. 27 (28), 1700769.
Han, X., et al., 2018. Anal. Chem. 90 (13), 8108–8115.
He, S., et al., 2020. J. Am. Chem. Soc. 142 (15), 7075–7082.
Huang, Y., et al., 2019. J. Mater. Chem. B 7 (2), 305–313.
Hyun, H., et al., 2015. Angew. Chem. Int. Ed. 54 (30), 8648–8652.
Hyun, H., et al., 2014. Angew. Chem. 126 (40), 10844–10848.
Jabs, D.A., et al., 2005. Am. J. Ophthalmol. 140 (3), 509–516.
Jalil, A., et al., 2012. Ocul. Immunol. Inflamm. 20 (4), 262–265.
Joseph, A., et al., 2020. Elife 9, e60547.
Kraft, J.C., Ho, R.J.Y., 2014. Biochemistry 53 (8), 1275–1283.
Kwon, H.-Y., et al., 2021. J. Am. Chem. Soc. 143 (15), 5836–5844.
Lardenoye, C.W., et al., 2006. Ophthalmology 113 (8), 1446–1449.
Li, P., et al., 2019. Chem. Sci. 10 (9), 2805–2810.
Li, W., et al., 2021. Anal. Chem. 93 (25), 8978–8985.
Luciano, M.P., et al., 2019. ACS Chem. Biol. 14 (5), 934–940.
Mavrofrides, E., et al., 2006. Retina 26 (6), 637–644.
Mellanby, R.J., et al., 2018. Chem. Sci. 9 (36), 7261–7270.
Mendive-Tapia, L., Vendrell, M., 2022. Acc. Chem. Res. 55 (8), 1183–1193.
Migacz, J.V., et al., 2022. Biomed. Opt Express 13 (3), 1755–1773.
Narayanan, R., et al., 2005. Curr. Eye Res. 30 (6), 471–478.
Noguchi, Y., et al., 2018. Can. J. Ophthalmol. 53 (4), e158–e162.
Notman, R., et al., 2006. J. Am. Chem. Soc. 128 (43), 13982–13983.
Pacheco, Y., et al., 2013. J. Immunol. 191 (5), 2072–2081.
Park, S.-J., et al., 2014. Stem Cell Res. 12 (3), 730–741.
Patel, A., et al., 2013. World J. Pharmacol. 2 (2), 47–64.
Penha, F.M., et al., 2013. PLoS One 8 (5), e64094.
Pescina, S., et al., 2018. J. Contr. Release 284, 84–102.
Robertson, M.J., et al., 2014. Nat. Protoc. 9 (4), 851–870.
Sakka, S.G., 2007. Curr. Opin. Crit. Care 13 (2), 207–214.
Samanta, A., et al., 2010. Chem. Commun. 46 (39), 7406.
Samanta, A., et al., 2011. Chem. Asian J. 6 (6), 1353–1357.
Sato, T., et al., 2018. Oxid. Med. Cell. Longev. 2018, 6065285.
Scott, J.I., et al., 2021. ACS Chem. Biol. 16 (8), 1304–1317.
Shirata, C., et al., 2017. Sci. Rep. 7 (1), 13958.
Sim, D.A., et al., 2015. Dis. Model Mech. 8 (11), 1479–1487.
Thavornpradit, S., et al., 2019. Theranostics 9 (10), 2856–2867.
Vendrell, M., et al., 2011. Org. Biomol. Chem. 9 (13), 4760–4762.
Wu, D., et al., 2019. Chem. Sci. 10 (29), 6944–6956.
Yam, H.-F., et al., 2003. Investig. Ophthalmol. Vis. Sci. 44 (1), 370–377.
Yraola, F., et al., 2004. QSAR Comb. Sci. 23 (23), 145–152.